A Pro-Regenerative Environment Triggers Premalignant to Malignant Transformation of Senescent Hepatocytes

Anna Wuestefeld[1], Viktoriia Iakovleva[1], Shirlyn Xue Ling Yap[1], Agnes Bee Leng Ong[1], Daniel Q. Huang[2,3], Timothy Wai Ho Shuen[4], Han Chong Toh[4], Yock Young Dan[2,3], Lars Zender[5,6,7], and Torsten Wuestefeld[1,8,9]

ABSTRACT

Unfortunately, available liver cancer treatments are associated with modest survival advantage. The biggest factor improving survival is early detection, but the current understanding of early transformation events is limited. Therefore, we set up a model to study these early events and investigated the relationship of premalignant, senescent hepatocytes, a regenerative environment, and the influence of secreted factors on liver tumorigenesis. Oncogene-induced senescence (OIS) was triggered in a subset of mouse hepatocytes, which under normal conditions, are eliminated by immunosurveillance. Inducing liver damage and regeneration was sufficient to trigger immunosurveillance escape of OIS hepatocytes, resulting in premalignant to malignant transformation and hepatocellular tumor development. Trefoil factor 3 (TFF3) was found to be overexpressed in OIS hepatocytes and in hepatocellular carcinoma. TFF3 deficiency strongly attenuated malignant transformation by increasing insulin-like growth factor binding protein 5 (IGFBP5) expression, which consequently dampened IGF receptor signaling. Furthermore, analysis of precancerous liver tissue validated TFF3 as an early liver cancer biomarker. Altogether, these findings provide mechanistic insights into early transformation and immunosurveillance escape in liver cancer, revealing TFF3 and IGFBP5 to be important players with opposite roles in tumorigenesis.

Significance: Liver damage induces a compensatory regenerative response that can drive premalignant to malignant transformation of senescent hepatocytes.

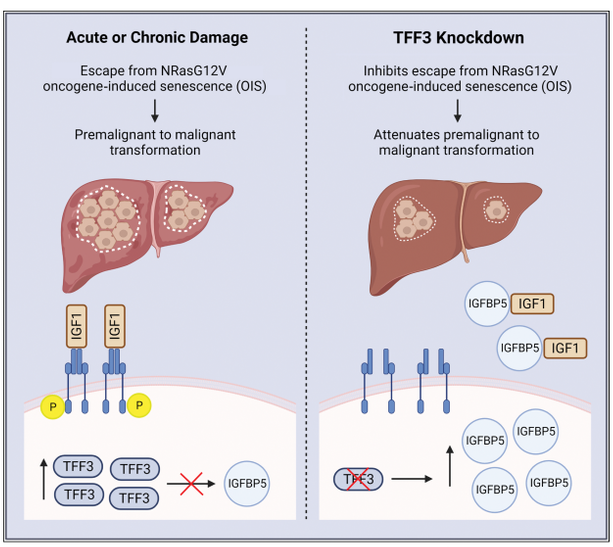

[1]Laboratory of In Vivo Genetics & Gene Therapy, Genome Institute of Singapore, Singapore. [2]Department of Medicine, Yong Loo Lin School of Medicine, National University of Singapore, Singapore. [3]Division of Gastroenterology and Hepatology, University Medicine Cluster, National University Hospital, Singapore. [4]Department of Medical Oncology, National Cancer Centre Singapore, Singapore. [5]Department of Medical Oncology and Pneumology (Internal Medicine VIII), University Hospital Tuebingen, Tübingen, Germany. [6]Cluster of Excellence 'Image Guided and Functionally Instructed Tumor Therapies' (iFIT), Eberhard Karls University of Tübingen, Tübingen, Germany. [7]German Consortium for Translational Cancer Research (DKTK), Partner Site Tübingen, German Cancer Research Center (DKFZ), Heidelberg, Germany. [8]National Cancer Centre Singapore, Singapore. [9]Nanyang Technological University, School of Biological Sciences, Singapore.

Corresponding Author: Torsten Wuestefeld, Laboratory of In Vivo Genetics & Gene Therapy, Genome Institute of Singapore, Singapore. Phone: 656-808-8218; E-mail: wustefeldt@gis.a-star.edu.sg

Cancer Res 2023;83:428–40

doi: 10.1158/0008-5472.CAN-22-1477

Introduction

Hepatocellular carcinoma (HCC) is the fourth most common cause of cancer-related death worldwide (1). Unfortunately, it is one of the few neoplasms with a steady increase in both incidence and mortality (2). Liver cancer is intrinsically chemoresistance and has so far no specific molecular targets for treatment or molecular markers for patient stratification. The only curative treatment is tumor resection or liver transplantation, which is only applicable for early stages of the disease. Since 2020, the new FDA-recommended first-line therapy is a drug combination of VEGF receptor inhibitor and an antibody that blocks programmed death-ligand 1 with an overall survival advantage of roughly a year. These limited treatment outcomes clearly show the urgent demand for new therapies for HCC.

We used a unique acute/chronic liver damage model to identify potential therapeutic targets involved in early liver cancer development (**Fig. 1A**). Our approach has several stages and covers all essential steps during liver carcinogenesis. The first stage is entering cellular senescence. The cellular senescence program induces a state of stable cell-cycle arrest, which acts as an important barrier against tumor development (3–6). Senescence is not a purely passive proliferative arrest. Instead, senescent cells influence their environment

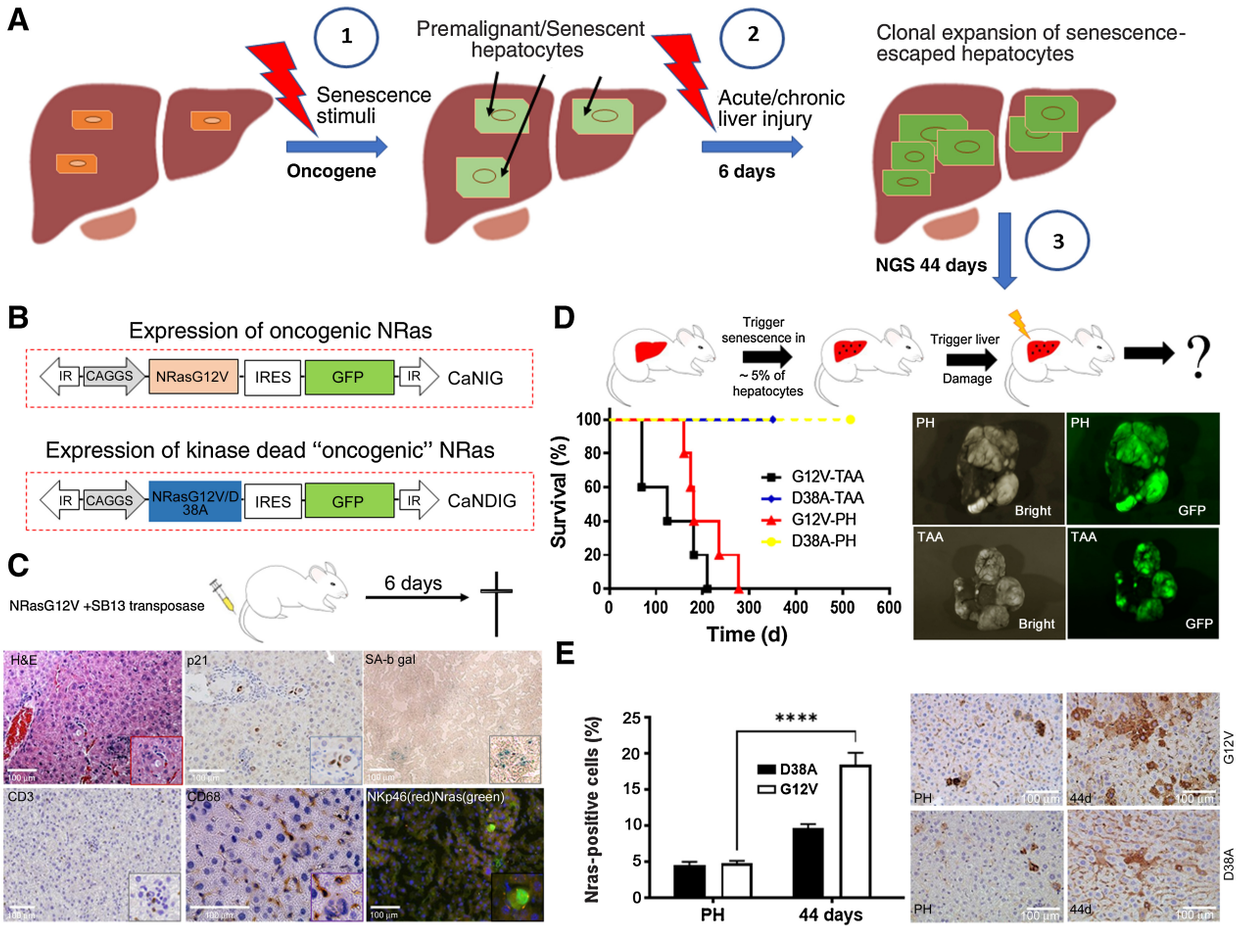

Figure 1.

In vivo oncogenic-induced senescence escape model. **A,** Mouse model to identify early specific molecular targets for liver cancer: 1, senescence stimuli (NRas); 2, liver injury/regeneration triggers premalignant to malignant transformation of senescent hepatocytes; 3, time point for RNA sequencing analyses to identify early molecular targets for liver cancer. **B,** Schematic representation of transposable element for stable intrahepatic gene expression of oncogenic NRas (NRasG12V) or an effector loop mutant (NRasG12V/D38A) and the marker gene GFP. **C,** OIS (indicated by H&E staining of senescent hepatocyte, by SA-β-gal and p21 staining) and immune surveillance (shown by staining for the T-cell marker CD3, macrophage and monocyte marker CD68, and NK cell marker NKp46) at 6 days post injection. **D,** Mice from experimental group (G12V, $n = 5$) and control group (D38A, $n = 4$) were either treated with TAA or mice from experimental group (G12V, $n = 5$) and control group (D38A, $n = 6$) underwent PH (4). Kaplan–Meier survival curves are shown. Right, macroscopic pictures of the liver with visible tumors as well as GFP scans are shown. G12V, CaNIG-NRasG12V; D38A, CaNIG-NRasD38A. **E,** Quantification analyses of NRas-positive hepatocytes at 44 days after PH. An expansion of NRas-positive cells can be detected (****, $P < 0.0001$). Shown are NRas stainings of representative liver slides (×200 magnification), 10 optical fields per animal ($n = 5$) for each group.

through an active secretory program known as the senescence-associated secretory phenotype (SASP; refs. 7–9). SASP includes various cytokines and growth factors, and it was reported that this 'secretory phenotype' can have pro- as well as antitumorigenic effects. In fact, it was shown that oncogene-induced premalignant senescent hepatocytes secrete chemo- and cytokines, triggering immune-mediated clearance of these cells (8, 10). The oncogene-mediated form of senescence in cells is called oncogene-induced senescence (OIS). OIS has a tumor suppressive function by preventing uncontrolled cell proliferation. Interestingly, senescent cells, along with apoptotic cells, are detected more abundantly in premalignant lesions compared with established malignant tumors (5). In our mouse model we triggered oncogene expression in a subset of hepatocytes, which resulted in OIS premalignant cells.

The second stage is senescence escape, which is associated with proliferation of senescence-escaped hepatocytes, immune evasion, and leads to liver tumor development. It is known that preneoplastic lesions frequently progress to malignant tumors, implying that molecular alterations during carcinogenesis eventually overcome OIS (11, 12). Interestingly it was shown that cells also escape other forms of senescence, reenter the cell cycle and proliferate. For example, senescent liver cells are able to repopulate the liver of fumarylacetoacetate hydrolase–deficient mice (13) and embryonic senescent cells can contribute to tissues after birth (14). In the process of tumorigenesis, senescence escape might be an early and essential step. In our mouse model, we triggered senescence escape by inducing acute/chronic liver damage. This step reflects premalignant to malignant transition.

At the last stage, we simply monitored immunosurveillance escape and premalignant to malignant transformation of the hepatocytes resulting in full tumor development.

Our approach reflects the whole cancer trajectory, covering early clonal expansion and immune evasion, premalignant to malignant transformation and full tumor development. Because our chimeric cancer mouse model is able to recapitulate cancer development from precancerous cells surrounded by normal cells in an immune-competent environment, it allows the identification of new therapeutic intervention points. Furthermore, identified targets could be used to develop RNAi based treatments.

Materials and Methods

Human samples

HCC human tissues samples of different etiology [HCC induced by hepatitis B virus (HBV), hepatitis C virus (HCV), or nonalcoholic steatohepatitis (NASH)], for validation of targets was provide by the Singapore Translational Cancer Consortium. Application is approved by SingHealth Tissue Repository Tissue Release Committee. The application reference number is 21-LIV-270. cDNA samples from cirrhotic liver tissue and healthy donors were provided by Huck Hui Ng's laboratory in Genome Institute of Singapore.

Mouse models

Mice, hydrodynamic injection, and thioacetamide administration

C57BL/6JInv 5 weeks old female mice (IMSR_JAX:000664) and C.B-17 SCID 5 weeks old female mice (C.B-Igh-1b/IcrTac-Prkdcscid) were purchased from InVivos. All mice were housed and maintained under pathogen-free conditions in accordance with the institutional guidelines of the Biological Resource Centre (BRC), A*STAR, Singapore. All animal experiments have been approved by the Institutional Animal Care and Use Committee (IACUC# 191452). Vectors for hydrodynamic tail vein (HDTV) injection (15) were prepared using the Qiagen EndoFreeMaxi Kit (Qiagen). For transposon mediated gene transfer, animals received a 5:1 molar ratio of transposon to transposase-encoding plasmid (30 μg total DNA). DNA was suspended in saline solution at a final volume of 10% of the animals 'body weight and injected via the tail vein in < 10 seconds. To induce chronic liver damage, thioacetamide (TAA) was delivered by intraperitoneal injections. Intraperitoneal administration of TAA was performed 3 times per week during 8 weeks with concentration of 40 mg/mL (100 μL of this solution for 20 g mouse), which was dissolved in saline solution.

Cell lines

Phoenix (CRL-3213), AML12 (CRL-2254), BNL CL.2 (TIB-73), Hep3B (HB-8064, RRID: CVCL_0326), HepG2 (CRL-11997, RRID: CVCL_3701), and SNU398 (CRL-2233) were purchased from ATCC cell products (www.atcc.org). Immortalized human hepatocytes-SV40 were purchased from Creative Bioarray (catalog no. CSC-I9016L). Human liver cancer derived primary cell lines (HCC 10.3, HCC 26.1). RNA samples of HCC 10.3, HCC 26.1 were provided by Wai Leong Tam's laboratory in Genome Institute of Singapore.

Generation of subcutaneous tumors

The HepG2 cell line was transduced by retroviruses expressing single short hairpin RNAs (shRNA; shNC, *shTff3*). After puromycin selection 2×10^6 cells were injected subcutaneously (rear flanks) on C.B-17 SCID (C.B-Igh-1b/IcrTac-Prkdcscid) mice. Subcutaneous tumors were isolated and measured (11) after 7 weeks.

Vector construction and shRNA cloning

The vectors pT/Caggs-NrasG12V-IRES-GFP, pT/Caggs-NrasG12V/D38A-IRES-GFP, and pPGK-SB13 have been described previously (10). The NrasG12V sequence in the transposon plasmid was first replaced by a polylinker. Next NrasG12V, c-myc, and Akt-1 were inserted by PCR cloning using primers with AscI, MluI, and NotI or AgeI restriction sites. GFP was added into transposon plasmids via PCR cloning using primers with NotI and AgeI restriction sites. The miR30 5′ sequence was inserted using AgeI and NheI. Individual shRNAs for validation experiments were designed using Biopred algorithms and synthesized as 97 bp oligos DNA (IDT, Integrated DNA Technologies, Singapore). The shRNAs were PCR cloned into MSCV plasmids using XhoI and EcoRI and shuttled into transposon plasmids using XhoI, MluI, and AscI fragments. The results of the cloning were verified by sequencing.

Two-thirds hepatectomy

Two-thirds (partial) hepatectomy was performed on C57BL/6JInv wild-type (WT) mice as described before (16). The median, right, and caudate liver lobes were surgically removed while mice were under general anesthesia.

Western blot

For Western blot analysis whole-cell extracts were prepared from mouse (AML12, BNL Cl.2), and human (HepG2) cell lines. Certain proteins were isolated from supernatant collected from HepG2 cells. The nuclear protein isolation was performed using Abcam Nuclear Extraction Kit (ab113474). Proteins were separated on a 10% or 4% to 20% gradient Mini-PROTEAN TGX Precast Protein Gels (Bio-Rad). The anti–trefoil factor 3 (TFF3) antibody (Thermo Fisher Scientific PA5–21081) was used at 1:500, the anti–insulin-like growth factor receptor 1 (IGFR1; phospho Y1161) antibody (Abcam AB_731544) was used at 1:100, the anti–insulin-like growth factor binding protein 5 (IGFBP5) antibody (Thermo Fisher Scientific PA5–37369) was used at 1:1,000, anti-Histone H3 antibody (Abcam AB_302613) was used at 1:1,000 and the anti-AFP, anti-tubulin, anti-GFP, or β-actin antibody (Cell Signaling Technology, #2137; Cell Signaling Technology, #9099; Cell Signaling Technology, #2956; Cell Signaling Technology, #4967) were used at a 1:2,000 dilution.

Protein array

Whole-cell protein extracts were prepared from mouse tissue samples and protein array was done using mouse cytokine antibody array kit (Abcam ab169820) and mouse growth factor array (RayBiotech C2). The procedures were done according to the manufacturer's instructions.

Histopathology

Histopathologic evaluation of murine liver and liver carcinomas was performed on hematoxylin and eosin (H&E)–stained paraffin sections by board certified pathologists [Advanced Molecular Pathology Laboratory (AMPL) IMCB, A*STAR, Singapore]. H&E, CD3 (1:100, AB_443425), CD68 (1:200, AB_307338) staining, and IHC for IGFBP5 (1:50, Thermo Fisher Scientific PA5–37369), N-Ras (1:100, AB_628041), p21 (1:25, AB_396415), ASGR1 (1:100, Thermo Fisher Scientific AB_2638286) staining were performed on paraffin-embedded liver sections by AMPL. Sections of snap-frozen

tissues were subjected to Ki67 (1:200, AB_443209), N-Ras (1:50, AB_628041), IGFBP5 (1:100, Thermo Fisher Scientific PA5–37369), NKp46 (1:50, AB_10552740), TFF3 (1:50, Thermo Fisher Scientific PA5–21081), pIGFR1 (1:100, Abcam AB_731544), p21 (1:50, AB_396415) stainings. Cells from mouse liver cell line (AML12) were stained with phospho-H2A.X pSer140 antibody (1:250, Thermo Fisher Scientific AB_559491). Human liver cancer cell line (HepG2) were stained with IGFBP5 (1:100, Thermo Fisher Scientific PA5–37369). SA-β-gal staining was performed using Senescence β Galactosidase Staining Kit (Cell Signaling Technology, #9860). Alexa Fluor 594 and 488 (Thermo Fisher Scientific, #R37117; Thermo Fisher Scientific, #R37121; and Thermo Fisher Scientific, #R37120; Thermo Fisher Scientific, #R37116)-conjugated secondary antibodies were used for signal detection. Microscopic analyses were performed using Observer Z1 microscope (Zeiss). Five high power fields were counted on two liver sections from each mouse liver (200X, >200 counted cells per field).

In vitro knockdown tests

Production of retroviral particles was accomplished using Phoenix packaging cells. The Phoenix cells were transfected with retroviral DNA via calcium phosphate–mediated transfection. The viral supernatant was applied directly on BNL CL.2 cells (for *Tff3-*, *Igfbp5-*) and human liver tumor HepG2 cells (for *hTFF3-*) for knockdown tests. Polybrene was added (1–10 μg/mL) to enhance infection efficiency. Target cells were selected using puromycin (1–10 μg/mL) and expanded or harvested for the preparation of whole-cell protein extracts or isolation of RNA.

Oxidative stress–induced senescence in AML12 cells

The mouse liver cell line AML12 was grown in DMEM containing 10% FCS and antibiotics (100 U/mL penicillin, 100 μg/mL streptomycin). Cells were seeded in 6-well plates at a density of 5×10^5 per well and allowed to adhere overnight before treatment. Cells were incubated with 0.5 mmol/L H_2O_2 in culture media for 60 minutes to induce senescence (the optimal conditions that were determined for induction of senescence rather than apoptosis or death). Control AML12 cells were incubated in culture media alone. Cells were then washed 3 times with PBS and incubated at 37°C, 5% CO_2 for 5 days before observing cell morphology and assessing the senescent phenotype. The senescence phenotype was assessed using cell morphology, SA-β-gal activity, the presence of senescence-associated heterochromatic foci and SASP.

Starvation experiment using AML12 cells and HepG2

The mouse liver cell line AML12 and human liver cancer cell line HepG2 were grown in DMEM containing 10% FCS and antibiotics (100 U/mL penicillin, 100 μg/mL streptomycin). Cells were seeded in 6-well plates at a density of 5×10^5 per well and allowed to adhere overnight before treatment. Cells were incubated with 1% FBS (the optimal conditions that were determined for cell stress rather than apoptosis or death) in culture media for 24 hours to induce "environmental stress." Control AML12 and HepG2 cells were incubated in culture media alone. Cells were then washed 3 times with PBS and collected for whole-cell protein extracts to be analyzed by Western blot technique.

EdU cell proliferation assay

For EdU proliferation assay, we used Click-iT EdU Cell Proliferation Kit for Imaging, Alexa Fluor 594 dye from ThermoFisher (catalog no. C10339). We use mouse liver cell line BNL CL.2 and human liver cancer cell lines Hep3B, HepG2, and SNU398. The procedures were done according to the manufacturer's instructions. In case of supernatant treatment of human liver cancer cell lines, cells were treated 2 times overnight with a supernatant from BNL CL.2 cells with a stable expression of shRNAs against *Tff3* or none-coding shRNA. After that the EdU proliferation analyses were done.

mRNA expression, quantitative PCR analysis

mRNA was isolated from whole cells or liver tissue using Isolate II RNA Mini Kit (Bioline). mRNA gene expression were performed by next-generation sequencing (NGS) facility (Genome Institute of Singapore) and analyzed using Partek Genomics Suite 7.0 software. cDNA synthesis was done with qScript microRNA cDNA Synthesis Kit or with Illumina TruSeq DNA/RNA v2 kit for NGS. Quantitative qPCR was performed with SYBR Green Master Mix (Applied Biosystems). Values were normalized toward β-actin quantification. Sequence of primers used for quantitative qPCR could be found in Supplementary Table S1.

Statistical analysis

Cumulative survival of mice was assessed by Kaplan–Meier analysis and statistical significance was calculated using the log-rank test. Unless otherwise stated, for all other comparisons statistical significance was calculated using the unpaired two-tailed Student *t* test. P values < 0.05 were considered to indicate statistical significance. All statistical analyses were performed using GraphPad Prism 9 software. Error bars are represented as mean ± SEM if not otherwise indicated. Gene ontology (GO) analysis was done using Partek Flow.

Data and code availability

Raw data for this study were generated at Genome Institute of Singapore core facility. Derived data supporting the findings of this study are available from the corresponding author upon request. Raw count and FPKM values are provided in Supplementary Data.

Results

Oncogenic-induced senescence

We used a unique OIS escape model. Our model covers the stages of senescence, senescence escape and clonal expansion. We induce the premalignant stage in 4% to 8% of hepatocytes, which reside in an otherwise normal microenvironment. Schematic representation of the model is presented in **Fig. 1A**. We trigger OIS by stably delivering transposable elements expressing oncogenic NRas (NRasG12V) into hepatocytes *in vivo* using HDTV injection. Transposable elements encoding an effector loop mutant (NRasG12V/D38A), incapable of signaling to downstream pathways, served as a control (**Fig. 1B**). In both cases, we introduced our constructs to immune-competent C57Bl6 WT mice. Senescent cells were detected by H&E, p21, and SA-β-gal staining (**Fig. 1C**) 6 days post injection. At this time point, we have stable integration of our constructs in the genome. In immune-competent mice, senescent cells are eliminated through immune surveillance and therefore cannot be detected beyond 60 days of injection. As a result, WT mice do not develop liver tumors (10). Active immune surveillance is shown by the staining for the T-cell marker CD3, macrophage and monocyte marker CD68 and NK cell marker NKp46 (**Fig. 1C**) 6 days after HDTV injection. In contrast, microscopic examination of C.B-17 SCID mice livers harboring senescent hepatocytes did not show an inflammatory reaction with large clusters of immune cells

surrounding morphologically altered, senescent hepatocytes (Supplementary Fig. S1A).

Liver damage triggers senescence escape

We were interested to investigate the effect of liver damage on the phenotype of senescent cells and its impact on tumorigenesis, as most liver cancer arises in diseased liver. First, we examine the impact of chronic liver damage on a group of WT mice with senescent hepatocytes, using TAA treatment starting 6 days after OIS. At this point, the experimental and control group have similar number of cells with stable intrahepatic gene expression of oncogenic NRas. At later time points, time-course analysis revealed a rapid loss of Nras-positive cells due to immune clearance (10). Therefore, we performed TAA treatment of WT mice baring senescence hepatocytes at 6 days after OIS. Interestingly, chronic liver damage seems to trigger senescence escape, leading to multinodular liver tumors after latency (**Fig. 1D**). Macroscopic and microscopic analysis indicates that all tumor nodules are GFP positive. GFP expression is linked to NRasG12V expression, suggesting that tumors developed from OIS-escaped hepatocytes.

Next, we performed 2/3 partial hepatectomy (PH; ref. 16) to induce a singular massive acute liver damage in WT mice 6 days after OIS. At time of surgery (0 time point), we observed no difference in the basic proliferation rate (Ki67) in the liver among groups (Supplementary Fig. S1B). Moreover, the percentage of p21-positive cells in the OIS group was higher than the number for NRas-positive hepatocytes (**Fig. 1E**; Supplementary Fig. S1B). The control group expressing the kinase dead NRas (D38A) had the same amount of NRas-positive cells but no detectable levels of p21-positive cells (**Fig. 1E**; Supplementary Fig. S1B). This result supports the notion of paracrine senescence (8) on neighboring cells.

The senescent cells seem to attenuate proliferation 48 hours after PH (Supplementary Fig. S1C). Only in the setting with senescent hepatocytes, the proliferation rate decreased (Ki67) and cell cycle arrested p21-positive hepatocytes increased (Supplementary Fig. S1C). These results show that even with active immune surveillance, senescent cells have an effect on their microenvironment and can reduce the ability of the liver to proliferate. T.W. Kang (10) demonstrated that impaired immune surveillance of premalignant senescent hepatocytes results in the development of HCC. This suggests that without immune surveillance, some NRas expressing hepatocytes over time can escape the senescence program. Long term after acute liver damage, we observed similar results to chronic liver damage. The experimental groups of mice developed multinodular liver tumors (**Fig. 1D**). Remarkably, we were able to detect senescence escape indicated by clonal expansion of NRas-positive hepatocytes as early as 44 days after acute liver damage. The number of NRas-positive cells at 44 days post PH were significantly higher ($P < 0.0008$) in the OIS group compared with control and at least 4 times higher compared with the number of NRas-positive hepatocytes at the intervention time (**Fig. 1E**). Our result suggests that premalignant hepatocytes upon liver damage had escaped senescence arrest and immune surveillance, leading to the development of HCCs. In our pilot experiment we determined the number of NRas-positive hepatocytes at 16, 30, and 44 days post liver damage. We saw no decline in NRasG12V-positive hepatocytes at 16 days, indicating immune surveillance escape. In addition, significant clonal expansion was seen first at 44 days (Supplementary Fig. S1D). Therefore, we focused our further studies on 44 days post liver damage.

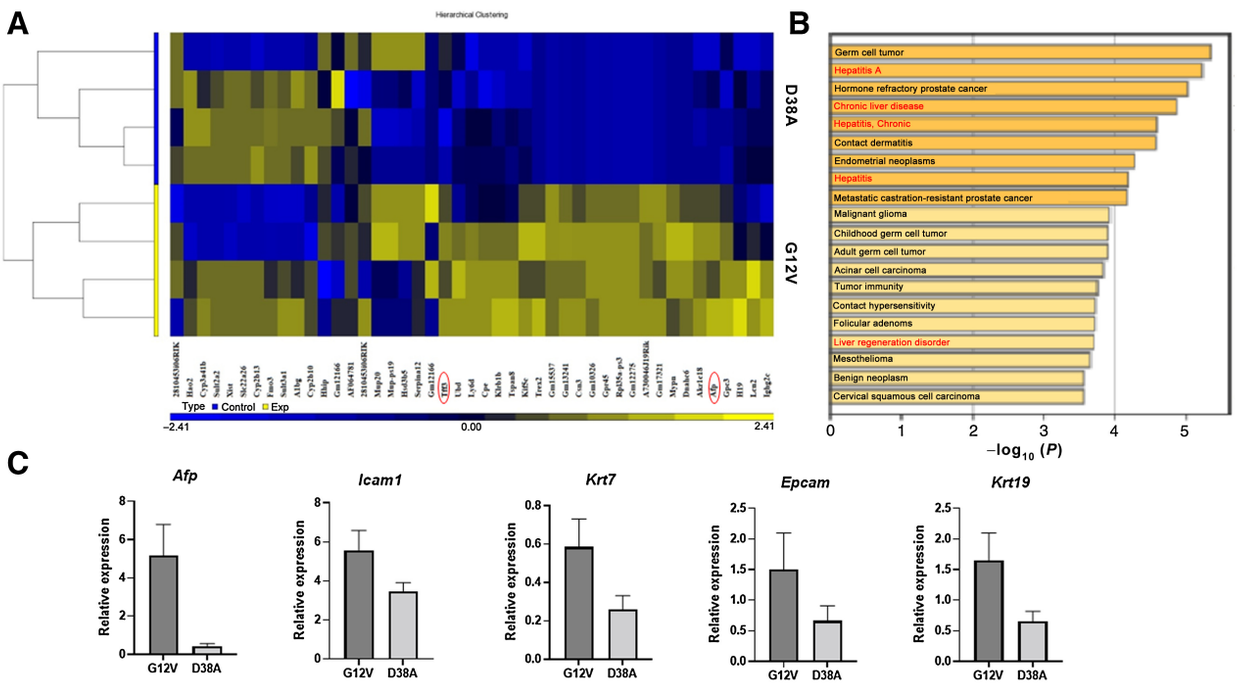

Figure 2.

Transcriptome heatmap based on NGS analyses. **A,** Transcriptome analysis 44 days post hepatectomy identifies a small number of signature genes (Shown are DEG with $P < 0.05$ and $\log_2$ fold > 1). G12V (CaNIG-NRasG12V) group compared with D38 (D38A, CaNIG-NRasG12VD38A) as control group. The focus was on protein coding genes (4 animals for each group, G12V vs. D38A). **B,** transcriptome analysis 44 days post hepatectomy identifies higher expression of signature genes that are strongly associated with hepatitis and cancer (GO analysis). **C**, Higher expression of oncofetal genes detected in experiment (G12V) compared with the control (D38).

Expression profile of hepatocytes during clonal expansion after acute liver damage

Clonal expansion of NRas-positive hepatocytes at 44 days after PH indicates some of the senescent hepatocytes escaped the senescence program. We detected a highly significant ($P < 0.0001$) increase in NRas-positive hepatocytes in liver tissue of WT mice injected with oncogenic NRas 44 days post PH compared with the control (∼18% vs. less than 10%, **Fig. 1E**). Therefore, we decided to use liver tissue from 44 days' time point to analyze the expression profile of liver. The data was statistically analyzed and we identified a set of genes (∼56 candidates) significantly ($P < 0.05$) upregulated in the experimental group (**Fig. 2A**). Importantly, among the differential expressed genes was α-fetoprotein (*Afp*). AFP is the most widely used tumor biomarker currently available for the early detection of HCC (17); hence, supports the transformative effect of liver damage/regeneration on senescent premalignant hepatocytes. Furthermore, the transcriptome analysis identifies signature genes that are strongly associated with hepatitis and cancer (GO analysis, **Fig. 2B**). Marker genes for hepatoblasts are also higher expressed, indicating fetal reprogramming (**Fig. 2C**). We went on to validate differential gene expression for several candidates by RT-PCR. We tested the expression in the context of progressive disease in our mouse model and in human hepatocytes, HepG2 human liver cancer cells and human liver cancer derived primary cell lines. This qPCR analysis validated differential expression of *Tff3*, tetraspanin 8 (*Tspan8*), carboxypeptidase E (*Cpe*), glypican 3 (*Gpc3*), and ubiquitin D (*Ubd*). We were able to detect low expression levels of *Tff3*, *Tspan8*, *Cpe*, *Gpc3*, and *Ubd* already at the OIS stage before acute liver damage. However, the expression level for all genes increased at 44 days after acute liver damage and was even higher in HCC tumors (developed as a result of senescence escape). We also confirmed higher expression level of the same genes in human liver cancer cell line (HepG2) and human liver cancer derived primary cell lines (HCC 10.3, HCC 26.1). Expression level in human liver cancer cells was compared with the one in human immortalized hepatocytes (Supplementary Fig. S2). Using this validation step, we can see a disease related expression pattern, which is evolutionary conserved. Interestingly, some of the identified targets are already upregulated in cirrhotic liver tissue (Supplementary Fig. S3A), supporting the point of being early disease marker.

We then proceeded with further validation on the contribution of the identified genes to tumor development. We first probed for *Tff3* as TFF3 is a secreted protein and a member of the trefoil family. Interestingly, from the family of three TFFs, only higher expression of *Tff3* was observed (Supplementary Fig. S3B). Under healthy conditions, TFF3 is mainly expressed in gastrointestinal mucosa (NCBI). However, TFF3 overexpression is frequently observed in human cancers, including human gastric cancer (18), skin carcinoma (19), and breast cancer (20), and it is thought to induce cancer cell growth. We confirmed higher expression of TFF3 in human HCC compared with the expression in healthy liver tissue. We observed TFF3 expression in human HCC samples associated with hepatitis B, C, and nonalcoholic steatohepatitis (Supplementary Fig. S3C).

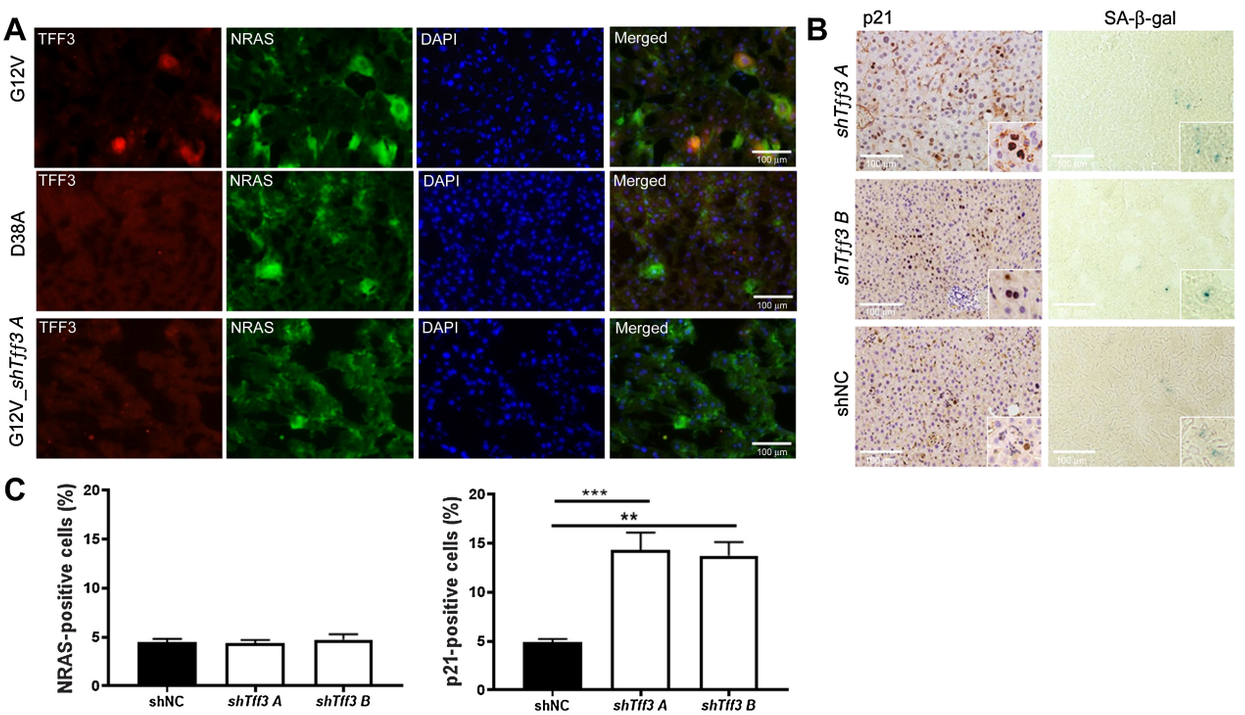

Figure 3.

TFF3 is specifically expressed in OIS hepatocytes and its knockdown does not affect senescence. **A,** IHC staining (×200 magnification) of liver tissues from WT mice injected with either CaNIG-NRasG12VD38A ($n = 6$), CaNIG-NRasG12V ($n = 5$), or CaNIG-NRasG12V–*shTff3 A* ($n = 4$). Co-staining against TFF3 and NRas shows that TFF3 is colocalized with NRas in senescent hepatocytes (top). Bottom panel shows efficient knockdown of *Tff3* (CaNIG-*shTff3 A*), indicated by no detection of TFF3. **B,** NRasG12V-mediated OIS indicated by SA-β-gal and p21 staining in mice injected with either CaNIG-NRas-*shTff3A* ($n = 4$), CaNIG-NRas-*shTff3B* ($n = 5$), or CaNIG-NRasG12V-shNC ($n = 5$). **C,** Quantification of NRas and p21-positive hepatocytes. Mice injected with either CaNIG-NRas-*shTff3A* ($n = 4$), CaNIG-NRas-*shTff3B* ($n = 5$), or CaNIG-NRasG12V-shNC ($n = 5$) underwent PH 6 days post injection (p21 counting). **, $P < 0.01$; ***, $P < 0.001$.

Expression profile of *Tff3* during senescence

We first verified the expression by qPCR in the liver with OIS hepatocytes before liver damage. *Tff3* expression was 2.7 fold higher in livers of the experimental group (Supplementary Fig. S2). Furthermore, specific co-staining for TFF3 and NRas on tissue slides proves the colocalization of TFF3 with senescence inducing NRasG12V but not with the kinase dead mutant (**Fig. 3A**). We then checked if increased TFF3 expression is specific for NRas induced OIS. We detected higher expression of TFF3 by Western blot during oxidative stress–induced senescence (OSIS) in a non-transformed mouse hepatocyte cell line (AML12). Senescence was confirmed by staining for indicator of direct DNA-damage phospho-H2A.X and senescence marker SA-β-gal (Supplementary Fig. S4A). In addition, we induced cellular stress by serum starvation (1% FBS) on AML12 and HepG2 cells. We detected no upregulation of TFF3 expression in AML12 and HepG2 (Supplementary Fig. S4B). This indicates that senescence is important to trigger strong TFF3 induction.

We continued to investigate the role of TFF3 during senescence and tumor development. We designed two independent shRNAs against *Tff3* (*shTff3 A* and *shTff3 B*). The efficiency of *Tff3* knockdown was confirmed using RT-PCR (Supplementary Fig. S4C). As a control, we used two independent nontargeting shRNAs (shNC A and shNC B). OIS was induced in three different groups of WT mice using oncogenic NRas together with shRNAs against *Tff3* (*shTff3 A* and *shTff3 B*) and nontargeting shRNA (shNC B) as control. Constructs were delivered together with a plasmid coding for transposase SB13 by HDTV injection as described previously (10). Senescence induction was confirmed by staining for p21 and SA-β-gal (**Fig. 3B**). Six days after HDTV injection, we performed 2/3 PH to induce acute liver damage. At 0 time point (resected liver tissue), we did not observe any difference in the amount of NRas-positive cells between groups. However, the amount of arrested p21-positive hepatocytes was strongly increased to 14% in case of *Tff3* knockdown ($P < 0.001$ and $P < 0.0039$ respectively) compared with 5% in the control shNC (**Fig. 3C**). Importantly the expression of the control shRNA did not affect the amount of NRas and p21-positive cells compared with expression of NRas without shRNA (see **Figs. 1** and **2**; Supplementary Fig. S1B). This result indicates that cells with *Tff3* knockdown have a stronger paracrine effect inducing an increase of p21-positive cells. Interestingly, 48 hours after PH, we observed an even stronger increase ($P < 0.0005$) of p21-positive hepatocytes in the *Tff3* knockdown group correlating with a decreased rate ($P < 0.0001$) of Ki67-positive hepatocytes (Supplementary Fig. S5A). This indicates that the increased amount of p21-positive cells attenuated proliferation of hepatocytes including NRas-positive hepatocytes in case of *Tff3* knockdown.

Knockdown of *Tff3* strongly attenuates premalignant to malignant transformation of senescent hepatocytes

Mice were injected with either a construct for the expression of oncogenic NRas and a shRNA targeting *Tff3* (two independent shRNAs were tested: *shTff3.A* & *shTff3.B*) or a nontargeting control shRNA (shNC). Six days post injection, acute liver damage was

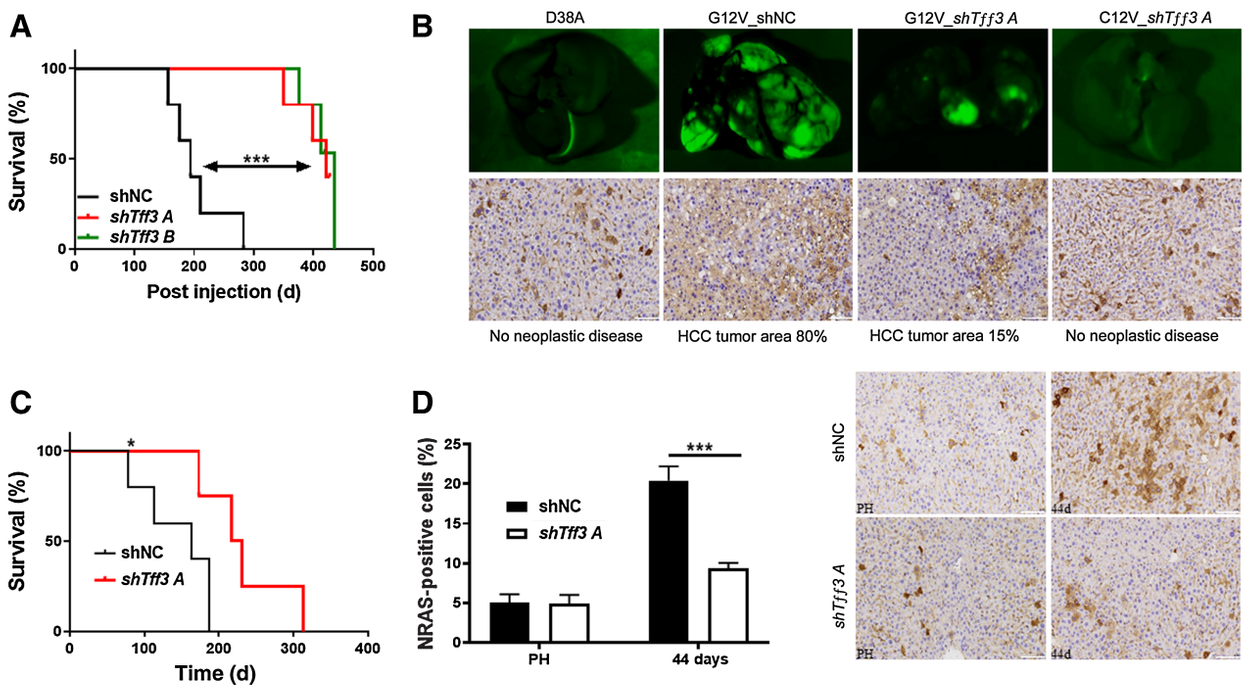

Figure 4.

Knockdown of *Tff3* strongly attenuates liver cancer. **A,** Kaplan–Meier survival curve of mice injected with CaNIG-NRas-*shTff3A* ($n = 5$), CaNIG-NRas-*shTff3B* ($n = 5$), or CaNIG-NRasG12V-shNC ($n = 5$) long term after PH (*shTff3 A* and *shTff3 B*). ***, $P < 0.0001$. **B,** Shown are macroscopic GFP scans of the liver with tumors being GFP positive (top) as well as DAB-based NRas-specific stainings (×200 magnification) of matched tissue samples. Scale bar, 100 μm. **C,** Kaplan–Meier survival curve of mice injected with CaNIG-NRas-*shTff3A* ($n = 4$) or CaNIG-NRasG12V-shNC ($n = 5$) long term after TAA treatment. *, $P < 0.05$. **D,** Quantification of NRas-positive hepatocytes at 0 time point and 44 days after 2/3 PH. ***, $P < 0.0002$. Mice injected with CaNIG-NRas-*shTff3A* ($n = 4$) or CaNIG-NRasG12V-shNC ($n = 4$). Shown are NRas stainings of representative liver slides (×200 magnification, 4 animals for each group). Scale bar, 100 μm.

induced by PH. Mice expressing oncogenic NRas and shNC developed HCCs in a similar time frame as mice that underwent this treatment but only expressed oncogenic NRas without shRNA. However, mice expressing a shRNA targeting *Tff3* developed HCCs significantly later ($P < 0.0001$; **Fig. 4A**). Furthermore 4 of 10 mice did not develop any tumors and were histopathologic indistinguishable from samples injected with an effector loop mutant (NRasG12V/D38A), incapable of signaling to downstream pathways (**Fig. 4B**; Supplementary Fig. S5B). We obtained similar results after chronic liver damage. In this case, 6 days post injection, animals were treated 3 times per week for 8 weeks with TAA. Similarly, *Tff3* knockdown strongly attenuated HCC development after chronic liver damage (**Fig. 4C**).

Consistent with the strong survival advantage expression of *shTff3* strongly inhibited oncogenic NRas driven clonal expansion after PH. (**Fig. 4D**).

Forty percent of mice with *Tff3* knockdown did not develop any tumors over the monitored time frame. Therefore, we hypothesized that the mice expressing oncogenic NRas together with *shTff3*, which developed tumors might have escaped *Tff3* knockdown. Consistent with our hypothesis, we detected TFF3 in the formed tumors (Supplementary Fig. S5C). A detailed co-staining showed that NRas and TFF3 colocalized in the same cells (Supplementary Fig. S5C). As expression of *shTff3* is linked to the expression of oncogenic NRas, the cells must have found a way to escape *Tff3* knockdown.

Tff3 knockdown efficiently inhibits cell proliferation in mouse and human through cell intrinsic and paracrine mechanism

Interestingly, knockdown of *Tff3* alone is sufficient to slow proliferation of immortalized mouse liver cells *in vitro* indicated by reduced EdU incorporation (**Fig. 5A**). We also generated two independent shRNAs with efficient knockdown targeting human *TFF3* (Supplementary Fig. S5D). Knockdown of *TFF3* in human liver cancer cell line HepG2 strongly attenuated proliferation (**Fig. 5B**), indicating that the effect of *TFF3* knockdown is conserved between these two species and that *TFF3* knockdown attenuates proliferation even in transformed cells. Motivated by the *in vitro* results we decided to investigate the ability of HepG2 cells to form subcutaneous tumors in case of *TFF3* knockdown *in vivo*. Immune-deficient (C.B-17 SCID) mice were injected subcutaneously with HepG2 cells. Experimental group was injected with HepG2 cells expressing shRNA against human *TFF3* (*shTFF3* huA), where control group was injected with HepG2-shNC. Seven weeks later, tumors were isolated and the average size of tumors in experimental group was significantly smaller ($P < 0.008$; Supplementary Fig. S6A). The impact of TFF3 in this setting also highlights the interventional potential, as knockdown of TFF3 in fully transformed cancer cells suppresses tumor growth. To test the real therapeutic potential of targeting *Tff3* for liver cancer therapy, we used one of the most aggressive and fast chimeric liver cancer mouse models. We delivered a transposon-based vector for the expression of a combination of oncogenic c-Myc and Akt (CaMIA) together with

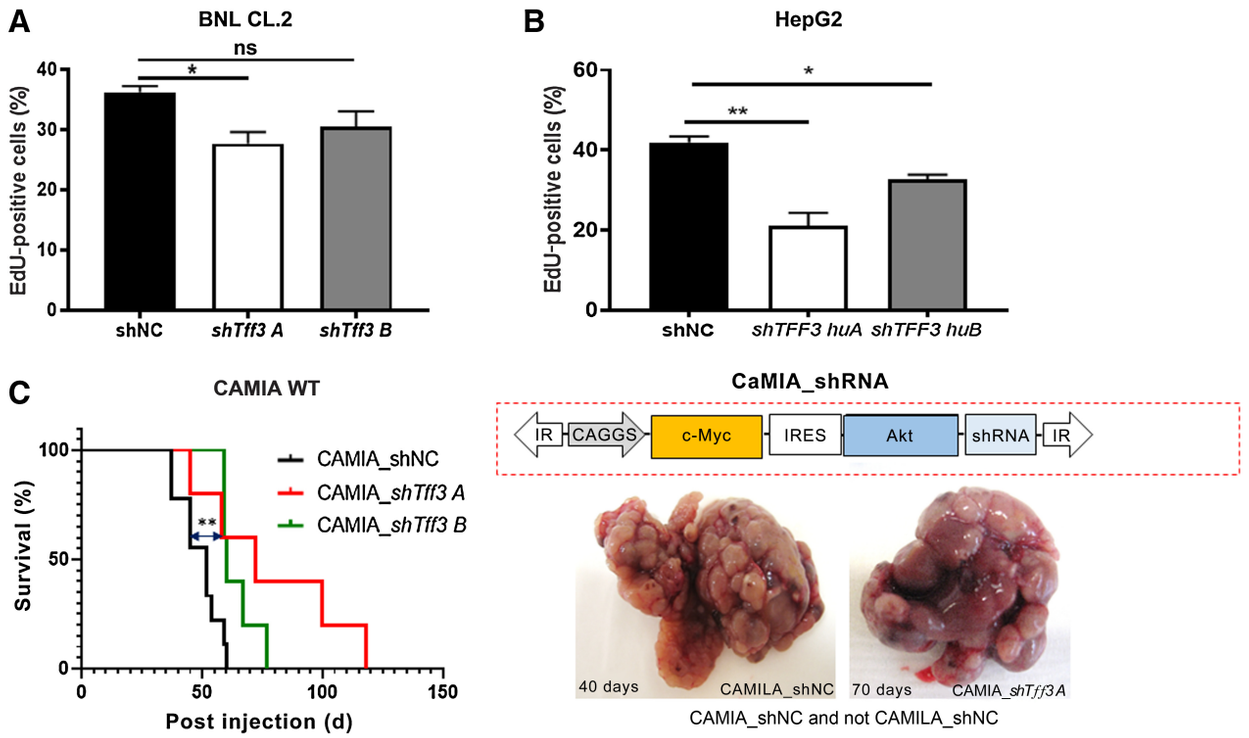

Figure 5.

The tumor suppressive effect of *Tff3* knockdown is independent of senescence. **A,** EdU incorporation assay (3 technical replicates, analyzing 5 different areas per replicate). Shown is the value of % EdU-positive cells ± SEM. BNL.CL2 cells with stable *shTff3 A*, *shTff3 B*, or shNC expression were used. *, $P < 0.0349$; ns, nonsignificant. **B,** EdU incorporation assay (3 technical replicates, analyzing 5 different areas per replicate). Shown is the value of % EdU-positive cells ± SEM. HepG2 cells with stable *shTFF3 huA*, *shTFF3 huB*, or shNC expression were used. *, $P < 0.0473$; **, $P < 0.011$. **C,** Schematic representation of transposable element for stable intrahepatic gene expression of the two oncogenes *c-Myc* and *Akt* together with either *Tff3* targeting shRNA (*shTff3 A* and *shTff3 B*) or control shRNA (shNC) on the right. Left, Kaplan–Meier survival curve of mice injected with CaMIA_shNC ($n = 9$), or CaMIA_*shTff3.*A and B, $n = 5$ mice each. **, $P < 0.007$. The two macroscopic light pictures on the right show examples of tumor burden for CaMIA_shNC at 40 days post injection and for CaMIA_*shTff3.*A at 70 days post injection.

either shNC or sh*Tff3* to the mouse liver by HDTV injection. In WT mice, the combination of those two oncogenic drivers led to a fast (∼50 days) tumor development. Even in this highly aggressive tumor model with two oncogenic drivers, *Tff3* knockdown significantly ($P < 0.007$) increased survival by attenuating liver cancer (**Fig. 5C**).

Our *in vivo* data indicated that *Tff3* knockdown increases paracrine inhibitory effects. To investigate the paracrine effect of *Tff3* knockdown on hepatocytes, we collected supernatant from mouse liver cell line expressing sh*Tff3* or shNC. The supernatant was used to treat different human liver cancer cell lines (Hep3B, HepG2, and SNU398). After two times treatment, we detected a significant reduction in EdU incorporation [Hep3B*** (p53-Null), HepG2** (p53-WT), SNU398**** (p53-Mutation)], indicating attenuation of cell proliferation (Supplementary Fig. S6B). No change was observed in case of supernatant from shNC-expressing cells. These results support a conserved mechanism between mouse and human, and highlight the impact of *TFF3* knockdown on cancer cell proliferation.

IGFBP5 is the mediator of *Tff3* knockdown paracrine effects

Tff3 knockdown induces a strong paracrine effect. First of all, in the liver tissue of mice where about 5% of hepatocytes express NRasG12V-shTff3 the amount of p21-positive cells was significantly higher compared with control (**Fig. 3C**). Especially in case of *Tff3* knockdown, in the same liver tissue, the amount of p21-positive cells was greater than the amount of NRas-positive hepatocytes. In addition, the supernatant from immortalized mouse embryonic liver cells with *Tff3* knockdown strongly attenuates cell growth even of human HCC cells (Supplementary Fig. S6B). To determine the factor or factors mediating these effects we performed a protein array using liver samples from these mice (**Fig. 6A**). Because the mediator of the observed paracrine effect has to be a secreted protein, we focused on changes in cytokines and growth factors. We found IFNγ, IGFBP5, IGFBP6, IL1β, IL2, and IL6 to be upregulated in G12V-s*hTff3A* liver tissues, secreted factors that were described before as part of the SASP. We focused on IGFBP5 as it showed a very strong *Tff3* knockdown-dependent increase. IGFBP5 is known to be upregulated during cellular senescence (21), irradiation-induced premature senescence and replicative senescence (22), indicating that it may not be OIS-specific. On another hand, it is known to be downregulated in different types of cancer tissue (23). In line with this, IGFBP5 was shown to have a tumor suppressor function (24). To validate our protein array results we performed immunofluorescence analysis and observed high expression of IGFBP5 during OIS in liver tissue with *Tff3* knockdown (**Fig. 6B**). Using the same samples and DAB (3,3′-diaminobenzidine) based IHC staining against IGFBP5, we detected significantly ($P < 0.0022$) higher amount of IGFBP5-positive cells in case of *Tff3* knockdown compared with control (**Fig. 6C**). Interestingly the knockdown of *Tff3* seems to influence the localization of IGFBP5 during OIS. We observed generally nuclear localization of IGFBP5 in samples with *shTff3* expression, where in controls mostly cytoplasmic localization was detected (**Fig. 6C** pictures). Our observation was supported by evaluation through a licensed pathologist. His report states that greater nuclear expression of IGFBP5 was found in NRasG12V-*shTff3A* and greater perinuclear labelling in NRasG12V-shNC. In addition, Western blot analysis of nuclear extracts (Supplementary Fig. S6C)

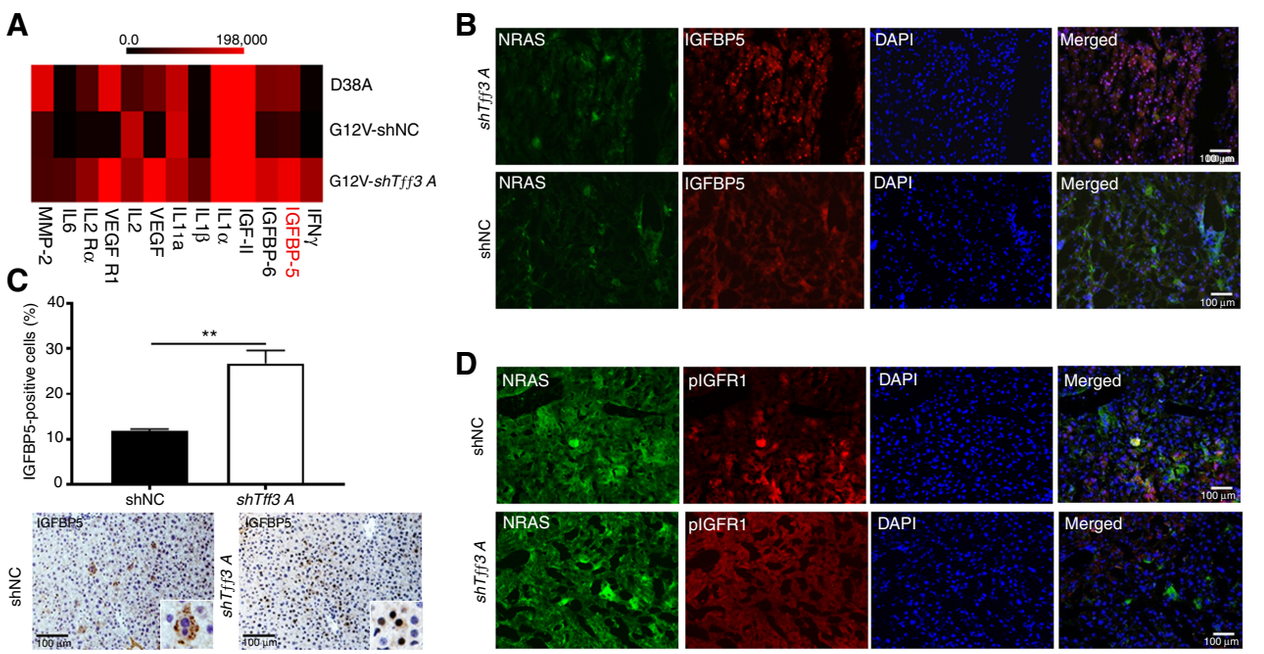

Figure 6.

Tff3 knockdown induces IGFBP5. **A,** Heatmap shows results for mouse cytokine antibody array. Whole-cell protein extracts from mouse livers with stable expression of either *shTff3 A* (G12V-*shTff3 A*), shNC (G12V-shNC), or an effector loop mutant (D38A) were analyzed (shown is the relative signal intensity). **B,** Immune fluorescence co-staining of mouse liver tissues against IGFBP5 and NRas 6 days after injection (×200 magnification). Mice injected with G12V-*shTff3 A* ($n = 4$) or G12V-shNC ($n = 4$). **C,** Quantification of IGFBP5-positive hepatocytes 6 days after injection. Mice injected with G12V-*shTff3 A* ($n = 4$) or G12V-shNC ($n = 4$). **, $P = 0.0022$. Representative DAB staining of mouse liver tissues shows localization of IGFBP5 during OIS (×200 magnification). **D,** Immune fluorescence staining of mouse liver tissues against pIGFR1 6 days after injection (×200 magnification). Mice injected with G12V-*shTff3 A* ($n = 4$) or G12V-shNC ($n = 4$).

isolated from HepG2 cells expressing *shTFF3* huA or shNC reveals higher nuclear expression of IGFBP5 in case of *TFF3* knockdown. Subcellular localization of IGFBP5 affects cell growth and migration of cancer cells (25). The nuclear localization and nuclear action of IGFBP5 is the molecular basis for several prominent IGF independent IGFBP5 activities (26).

Besides its intracellular function, IGFBP5 can be secreted and plays an important role in cell growth, survival, and differentiation by blocking the interaction between IGF and IGFR1 (27). As we observed paracrine effects, we decided to study the effect of *Tff3* knockdown on the activation of IGFR1. We delivered either NRasG12V with *shTff3* or shNC to the liver of mice. We then stained for NRas and activated IGFR1 (pIGFR1). Activation of IGFR1 was completely blocked by *Tff3* knockdown (**Fig. 6D**). Because IGFBP5 is known to bind with high affinity to circulating IGFs (28), our result suggests that IGFBP5 through binding to IGF1 prevents activation of IGFR1 in case of *Tff3* knockdown.

To further support the direct impact of *Tff3* knockdown on IGFBP5 levels and activation of IGFR1, we created three different mouse liver cell lines (BNL CL.2), with stable expression of two independent shRNAs against *Tff3* (*shTff3 A* and *shTff3 B*) and one expressing shNC. Western blot analyses revealed higher levels of IGFBP5 under *Tff3* knockdown, at the same time the levels of activated pIGFR1 were reduced (**Fig. 7A**). Similar results were obtained using human liver cancer cell line (HepG2; **Fig. 7B**), suggesting that the mechanism is conserved. In addition, it shows that *TFF3* knockdown induced IGFBP5 and the consequent inhibition of IGFR1 activation is independent of senescence. We also proved that IGFBP5 is secreted from human liver cancer cell line upon *TFF3* knockdown. High amounts of IGFBP5 were detected in supernatant collected from HepG2-sh*TFF3* cells (**Fig. 7C**). This is consistent with the detection of higher levels of IGFBP5 upon *TFF3* knockdown by using immunofluorescence staining for human IGFBP5 (**Fig. 7D**).

IGFBP5 is essential for maintaining senescence and suppression of premalignant to malignant transformation

To investigate the role of IGFBP5 during senescence, we designed shRNAs against it. The efficiency of *Igfbp5* knockdown was confirmed (Supplementary Fig. S7A). We then delivered transposon based constructs for the expression of oncogenic NRas and sh*Igfbp5* or shNC to the liver of mice. Six days later, livers were harvested and stained for senescence markers such as p21 and SA-β-gal (**Fig. 8A** and **B**). We did not observe any SA-β-gal–positive cells in samples with *Igfbp5* knockdown. In addition, we detected a strong reduction in p21-positive cells (Supplementary Fig. S7B), the number was lower than the amount of NRas-positive cells in the same samples (**Fig. 8C**). Furthermore, through immunofluorescence staining, we only detected NRas-

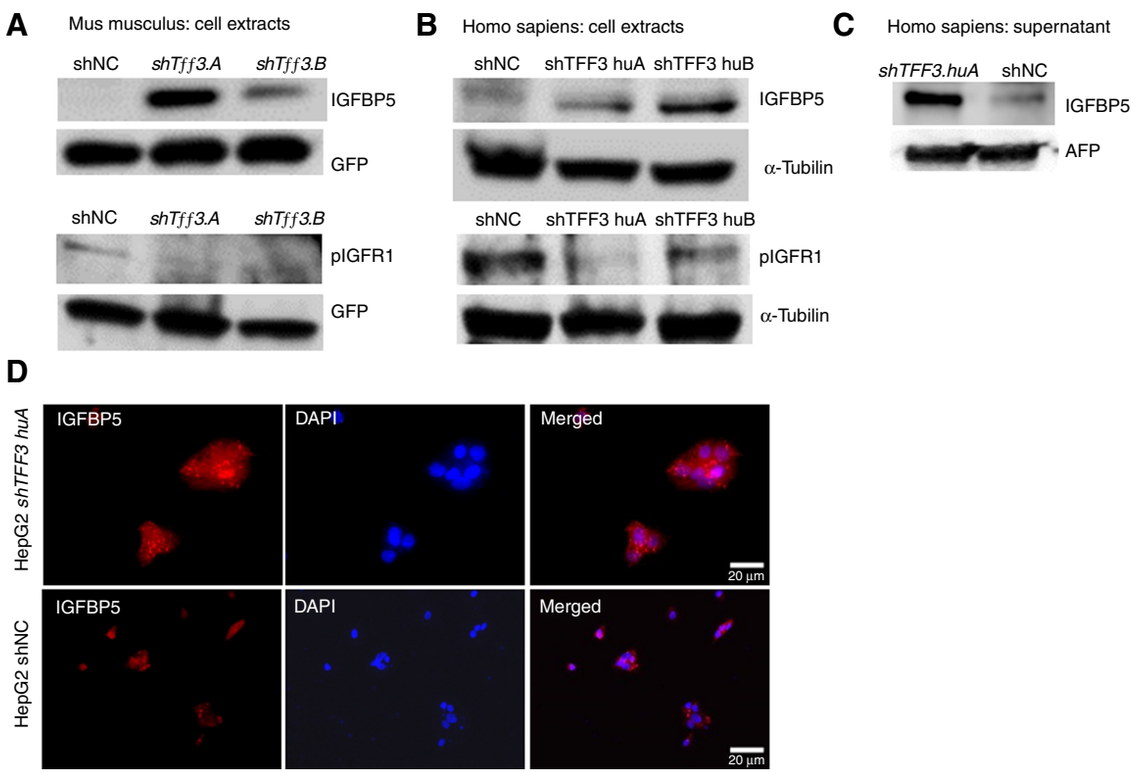

Figure 7.

Senescence independent *Tff3* knockdown induces IGFBP5, leading to attenuation of IGF signaling. **A,** Western blot analysis for the expression of IGFBP5 and pIGFR1 using protein extracts from immortalized mouse BNL CL.2 liver cells with stable *Tff3* knockdown (*shTff3 A* and *shTff3 B*) or control shRNA (shNC). GFP was used as a loading control because stable expression of shRNAs (shNC, *shTff3 A*, and *shTff3 B*) was linked to the expression of GFP. **B,** Western blot analysis for the expression status of IGFBP5 and pIGFR1 using protein extracts from human liver cancer cell line (HepG2) with stable *TFF3* knockdown (*shTFF3 huA* and *shTFF3 huB*) or control shRNA (shNC). Housekeeping gene α-tubulin was used as loading control. **C,** Western blot analysis for the secreted status of IGFBP5 protein using the supernatant from HepG2 cells expressing either shRNA against *TFF3* (*shTFF3 huA*) or control shRNA (shNC). Secreted AFP was used as loading control. **D,** Immunofluorescence staining against IGFBP5 using HepG2 cells expressing either *shTFF3 huA* or shNC (×200 magnification).

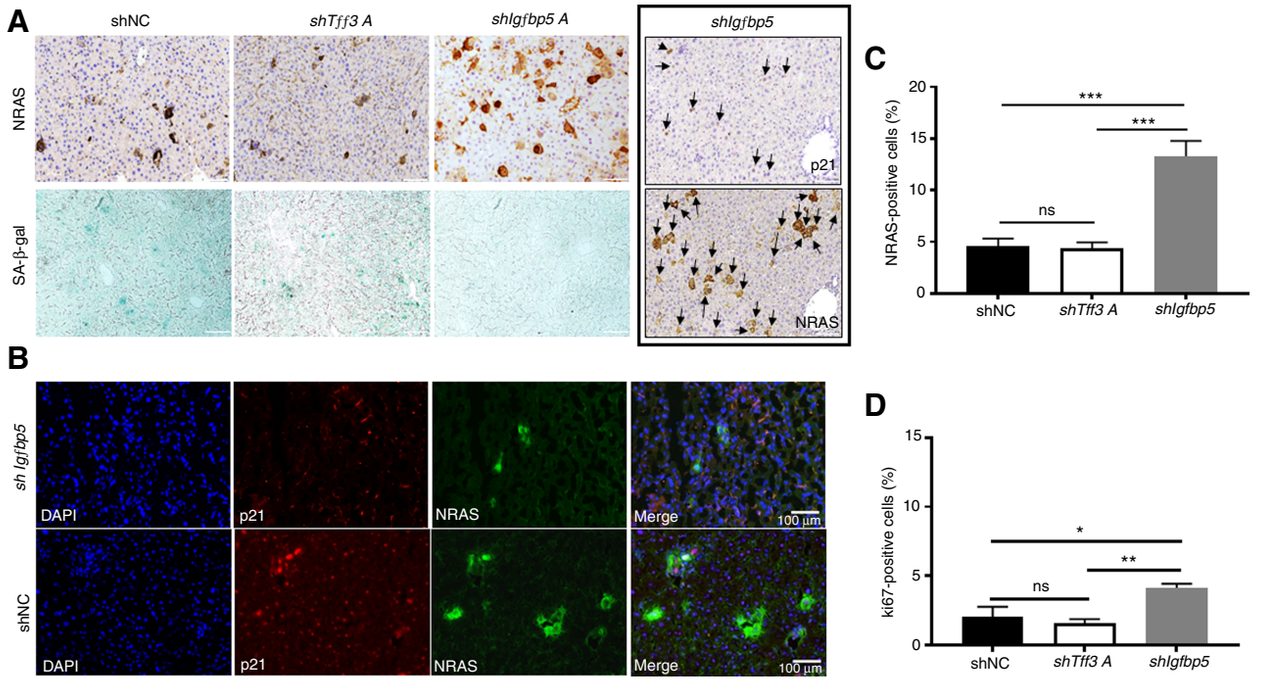

Figure 8.

Knockdown of *Igfbp5* suppresses OIS and leads to fast expansion of NRas-positive hepatocytes. **A,** DAB staining against NRas in mouse liver tissue with co-expression of oncogenic NRas and shRNA targeting *Igfbp5* (*shIgfbp5*, 5 mice) compared with liver tissue coexpressing oncogenic NRas and shRNAs targeting *Tff3* (*shTff3 A*; 4 mice) or nontargeting control shRNA (shNC; 5 mice) at 6 days post HDTV injection (×200 magnification). Scale bar, 100 µm. For the same samples SA-β-gal staining was used to detect senescent hepatocytes. Detected amount of NRas-positive cells and p21-positive cells in case of *Igfbp5* knockdown in the same area, by serial sections Arrows, NRas and p21-positive cells. Scale bar, 100 µm. **B,** Immunofluorescence co-staining for NRas and p21 in liver tissue of mice injected with G12V-*shIgfbp5* ($n = 5$) or G12V-shNC ($n = 5$). Liver tissues collected 6 days after PH. **C**, Quantification of NRas-positive hepatocytes 6 days after injection. Mice injected with G12V-*shIgfbp5* ($n = 5$), G12V-*shTff3 A* ($n = 4$), or G12V-shNC ($n = 5$). ***, $P < 0.0003$. **D,** Quantification of Ki67-positive hepatocytes 6 days after injection. Mice injected with G12V-*shIgfbp5* ($n = 5$), G12V-*shTff3 A* ($n = 4$), or G12V-shNC ($n = 5$). *, $P < 0.022$; **, $P < 0.0096$; ns, nonsignificant.

positive and at the same time p21-negative hepatocytes in samples with *Igfbp5* knockdown (**Fig. 8B**). DAB-IHC staining against NRas showed significant ($P < 0.0003$) increase of NRas-positive hepatocytes with sh*Igfbp5* already 6 days post injection (**Fig. 8C**). Consistent with this clonal cell expansion a significant increase in Ki67-positive cells was found (**Fig. 8D**). Taken together, increased proliferation coupled with the lack of SA-β-gal and strong reduction of p21-positive hepatocytes under *Igfbp5* knockdown, underline the importance of IGFBP5 expression for senescence induction.

Kang and colleagues (10) had shown that WT mice injected with oncogenic NRas do not develop liver tumors. To investigate if *Igfbp5* knockdown affects immune surveillance, a group of mice were injected with constructs for expression of oncogenic NRas and *shIgfbp5*. After ∼7 months, mice developed multinodular liver tumors (Supplementary Fig. S7C) and within 9 months all mice died from liver cancer. These results indicate that IGFBP5 is important in maintaining cellular senescence and suppressing premalignant to malignant transformation. Senescence represents an important barrier against tumor development, during which, IGFBP5 acts as an important tumor suppressor.

Discussion

In summary, we showed that liver damage, through the compensatory regenerative response, can drive premalignant to malignant transformation of senescent hepatocytes. We identified *Tff3* and *Igfbp5* to be important players with opposite roles in this process. On one hand, an increased production of *Tff3* supports cancer development by suppressing *Igfbp5*, on the other hand *Igfbp5* enforces senescence and suppresses tumor development. Interestingly, it was described before that both *Tff3* and *Igfbp5* are regulated by the IL6/gp130/STAT3 signaling pathway (22, 29–31). This signaling pathway is central for liver regeneration, but during persistent activation can also drive inflammation and cancer (32, 33). Our data suggest that the outcome of IL6/gp130/STAT3 signaling is dependent on the type of trigger. In the case of chronic inflammation vs. liver regeneration, the result of IL6/gp130/STAT3 signaling is either an *Igfbp5* dependent senescence induction or *Tff3*-dependent proliferation.

Furthermore, we identified *Tff3* as a therapeutic target for suppressing premalignant to malignant transformation and attenuating tumor growth of malignant hepatocytes. Suppression of *Tff3* induces IGFBP5, which in turn shows cell intrinsic and paracrine tumor suppressive effects. Intracellular we determined a shift to nuclear localization and it was described previously that nuclear localization of IGFBP5 plays an important tumor-suppressive role (24). In addition, IGFBP5 can be secreted to intercept IGFR ligands, thereby inhibiting the activation of IGFR and interfering with the IGF-IR pathway (Supplementary Fig. S7D) impacting cell growth, survival, and differentiation. Besides modulating these pathways, it was shown that the c-terminus of

IGFBP5 is able to inhibit angiogenesis and thereby suppressing tumor growth (24). In addition to these cancer-suppressive functions, it was shown that recombinant IGFBP5 can induce senescence in HUVEC cells (21), making IGFBP5 part of the paracrine senescence SASP factors. As recently brought up, the question is: "Are senescent cells friends or foes in cancer therapy?" (34). We can speculate, that changing the SASP composition by knocking down TFF3 and thereby inducing IGFBP5, makes the senescent cells friends. Under this condition important cancer pathways as IGF and PI3K-AKT signaling are suppressed, angiogenesis is inhibited and in the surrounding paracrine senescence, suppressing proliferation is induced. Therefore, *Tff3* knockdown establishes a cancer-suppressive microenvironment.

Our data clearly suggests the potential of developing RNAi based *anti-Tff3* therapies for liver cancer. Moreover, most of liver cancer is thought to arise from adult hepatocytes and many cancer cell lines continue to express the asialoglycoprotein receptor (ASGPR; Supplementary Fig. S7E). Given the rapid progression of RNAi-based therapeutics and the development of GalNAc modifications of siRNA, which allows for the efficient and specific uptake in hepatocytes via ASGPR, targeting *TFF3* represents a promising therapeutic approach with minimal toxic side effects.

Beside these direct mechanistic insides, the presented system is ideal to interrogate liver cancer development and immune escape. Liver cancer in the majority of cases arises on the background of chronic liver damage and cirrhosis (1). Chronic liver damage is associated with an increase in senescent cells over time, as is aging (35). By pure stochastics, prolonged damage increases the chances of oncogene activation and OIS. If damage and regeneration cycles continue, this can drive senescence escape. As was shown here, the slow expansion of the premalignant cells over time led to tumor formation.

We show that a single surgical removal of 2/3 of the liver is sufficient to drive senescence escape. Liver regeneration after PH is well described and leads to full liver recovery in around 2 weeks. Nevertheless, despite full regeneration, oncogenic NRas expressing senescence-escaped hepatocytes are no longer recognized by the immune system. The abrogation of immunosurveillance is an interesting area to investigate as it holds great insights into the interplay between immune escape response and cancer development.

For sure, we have to be cautious, as there are important differences between mice and men. First of all, most human HCCs are developing on the background of a cirrhotic liver, whereas in our mouse model we trigger OIS in a healthy liver microenvironment. Nevertheless, in our chimeric mouse liver we have local microenvironment changes due to the SASP. Importantly, we see an early embryonic hepatoblast like expression signature, when significant clonal expansion of the oncogene-expressing hepatocyte can be detected. This suggests fetal-like reprogramming, which was also recently described for HCC (36). Furthermore, we validated TFF3 as biomarker and therapeutic target not only in our mouse model, but also in human cells and patient samples. As mice and men are different, the most important step is to include human samples and/or humanized systems for vigorous validation

We validated TFF3 as a therapeutic target using both *in vitro* and *in vivo* approaches including various human liver cancer cell lines. Importantly, increased TFF3 expression in liver tumors seems independent from their etiology. We showed that in human tumors arising on the background of Hepatitis B or C, as well as under NASH conditions, higher levels of TFF3 can be identified. Even more we detected higher expression of *TFF3* in cirrhotic liver tissue, supporting the idea of *TFF3* being upregulated in premalignant stage of the disease. Altogether, our findings hold the promise that targeting TFF3 will have a profound effect in liver cancer.

Authors' Disclosures

A. Wuestefeld reports grants from NMRC during the conduct of the study. No disclosures were reported by the other authors.

Authors' Contributions

A. Wuestefeld: Conceptualization, data curation, formal analysis, validation, investigation, visualization, methodology, writing–original draft. **V. Iakovleva:** Validation, methodology. **S.X.L. Yap:** Data curation, validation, visualization, writing–original draft. **A.B.L. Ong:** Resources, data curation, validation, methodology. **D.Q. Huang:** Resources, data curation, methodology. **T.W.H. Shuen:** Resources, data curation, methodology. **H.C. Toh:** Resources, data curation, methodology. **Y.Y. Dan:** Resources, data curation, methodology. **L. Zender:** Resources, data curation, methodology. **T. Wuestefeld:** Conceptualization, resources, data curation, formal analysis, supervision, funding acquisition, writing–original draft, project administration.

Acknowledgments

The authors thank A*STAR AMPL for their assistance in pathological evaluations. They also thank A*STAR BRC for their assistance in animal housing. The research is supported by National Medical Research Foundation (NMRC/OFLCG/003b/2018; NMRC/CSA-SI/0013/2017; NMRC/OFIRG/0063/2017). Illustrations were created using Biorender.com.

The publication costs of this article were defrayed in part by the payment of publication fees. Therefore, and solely to indicate this fact, this article is hereby marked "advertisement" in accordance with 18 USC Section 1734.

Note

Supplementary data for this article are available at Cancer Research Online (http://cancerres.aacrjournals.org/).

Received May 6, 2022; revised September 16, 2022; accepted November 23, 2022; published first November 30, 2022.

Reference

1. Yang JD, Hainaut P, Gores GJ, Amadou A, Plymoth A, Roberts LR, et al. A global view of hepatocellular carcinoma: trends, risk, prevention, and management. Nat Rev Gastroenterol Hepatol 2019;16:589–604.
2. El-Serag HB, Kanwal F. Epidemiology of hepatocellular carcinoma in the United States: Where are we? Where do we go? Hepatology 2014;60:1767–75.
3. Chen Z, Trotman LC, Shaffer D, Lin H-K, Dotan ZA, Niki M, et al. Crucial role of p53-dependent cellular senescence in suppression of Pten-deficient tumorigenesis. Nature 2005;436:725–30.
4. Braig M, Lee S, Loddenkemper C, Rudolph C, Peters AHFM, Schlegelberger B, et al. Oncogene-induced senescence as an initial barrier in lymphoma development. Nature 2005;436:660–5.
5. Collado M, Gil J, Efeyan A, Guerra C, Schuhmacher AJ, Barradas M, et al. Tumor biology: senescence in premalignant tumors. Nature 2005;436:642.
6. Michaloglou C, Vredeveld LCW, Soengas MS, Denoyelle C, Kuilman T, van der Horst CMAM, et al. BRAFE600-associated senescence-like cell-cycle arrest of human nevi. Nature 2005;436:720–4.
7. Salama R, Sadaie M, Hoare M, Narita M. Cellular senescence and its effector programs. Genes Dev 2014;28:99–114.
8. Acosta JC, Banito A, Wuestefeld T, Georgilis A, Janich P, Morton JP, et al. A complex secretory program orchestrated by the inflammasome controls paracrine senescence. Nat Cell Biol 2013;15:978–90.
9. Collado M, Serrano M. Senescence in tumors: evidence from mice and humans. Nat Rev Cancer 2010;10:51–7.

10. Kang T-W, Yevsa T, Woller N, Hoenicke L, Wuestefeld T, Dauch D, et al. Senescence surveillance of premalignant hepatocytes limits liver cancer development. Nature 2011;479:547–51.
11. Milanovic M, Fan DNY, Belenki D, DÃ¨britz JHM, Zhao Z, Yu Y, et al. Senescence-associated reprogramming promotes cancer stemness. Nature 2018;553:96–100.
12. Yu Y, Schleich K, Yue B, Ji S, Lohneis P, Kemper K, et al. Targeting the senescence-overriding cooperative activity of structurally unrelated H3K9 demethylases in melanoma. Cancer Cell 2018;33:785.
13. Wang M-J, Chen F, Li J-X, Liu C-C, Zhang H-B, Xia Y, et al. Reversal of hepatocyte senescence after continuous *in vivo* cell proliferation. Hepatology 2014;60:349–61.
14. Li Y, Zhao H, Huang X, Tang J, Zhang S, Li Y, et al. Embryonic senescent cells reenter cell cycle and contribute to tissues after birth. Cell Res 2018;28:775–8.
15. Liu F, Song Y, Liu D. Hydrodynamics-based transfection in animals by systemic administration of plasmid DNA. Gene Ther 1999;6:1258–66.
16. Mitchell C, Willenbring H. A reproducible and well-tolerated method for 2/3 partial hepatectomy in mice. Nat Protoc 2008;3:1167–70.
17. Debruyne EN, Delanghe JR. Diagnosing and monitoring hepatocellular carcinoma with alpha-fetoprotein: new aspects and applications. Clin Chim Acta 2008;395:19–26.
18. Leung WK, Yu J, Chan FKL, To KF, Chan MWY, Ebert MPA, et al. Expression of trefoil peptides (TFF1, TFF2, and TFF3) in gastric carcinomas, intestinal metaplasia, and nonneoplastic gastric tissues. J Pathol 2002;197:582–8.
19. Hanby AM, McKee P, Jeffrey M, Grayson W, Dublin E, Poulsom R, et al. Primary mucinous carcinomas of the skin express TFF1, TFF3, estrogen receptor, and progesterone receptors. Am J Surg Pathol 1998;22:1125–31.
20. Balcer-Kubiczek EK, Harrison GH, Xu JF, Gutierrez PL. Coordinate late expression of trefoil peptide genes (pS2/TFF1 and ITF/TFF3) in human breast, colon, and gastric tumor cells exposed to X-rays. Mol Cancer Ther 2002;1:405–15.
21. Kim KS, Seu YB, Baek S-H, Kim MJ, Kim KJ, Kim JH, et al. Induction of cellular senescence by insulin-like growth factor binding protein 5 through a p53-dependent mechanism. Mol Biol Cell 2007;18:4543–52.
22. Sanada F, Taniyama Y, Muratsu J, Otsu R, Shimizu H, Rakugi H, et al. IGF binding protein-5 induces cell senescence. Front Endocrinol 2018;9:53.
23. Gullu G, Karabulut S, Akkiprik M. Functional roles and clinical values of insulin-like growth factor binding protein 5 in different types of cancers. Chin J Cancer 2012;31:266–80.
24. Hwang JR, Cho Y-J, Lee Y, Park Y, Han HD, Ahn HJ, et al. The C-terminus of IGFBP5 suppresses tumor growth by inhibiting angiogenesis. Sci Rep 2016;6:39334.
25. Akkiprik M, Hu L, Sahin A, Hao X, Zhang W. The subcellular localization of IGFBP5 affects its cell growth and migration functions in breast cancer. BMC Cancer 2009;9:103.
26. Xu Q, Li S, Zhao Y, Maures TJ, Yin P, Duan C, et al. Evidence that IGF binding protein-5 functions as a ligand-independent transcriptional regulator in vascular smooth muscle cells. Circ Res 2004;94:E46–54.
27. Beattie J, Allan GJ, Lochrie JD, Flint DJ. Insulin-like growth factor binding protein 5 (IGFBP5): a critical member of the IGF axis. Biochem J 2006;395:1–19.
28. Hwa V, Oh Y, Rosenfeld RG. The insulin-like growth factor binding protein (IGFBP) superfamily. Endocr Rev 1999;20:761–87.
29. Jiang G-X, Zhong X-Y, Cui Y-F, Liu W, Tai S, Wang Z-D, et al. IL-6/STAT3/TFF3 signaling regulates human biliary epithelial cell migration and wound healing *in vitro*. Mol Biol Rep 2010;37:3813–8.
30. Tebbutt NC, Giraud AS, Inglese M, Jenkins B, Waring P, Clay FJ, et al. Reciprocal regulation of gastrointestinal homeostasis by SHP2 and STAT-mediated trefoil gene activation in gp130 mutant mice. Nat Med 2002;8:1089–97.
31. Kojima H, Kunimoto H, Inoue T, Nakajima K. The STAT3–IGFBP5 axis is critical for IL6/gp130-induced premature senescence in human fibroblasts. Cell Cycle 2012;11:730–9.
32. Schmidt-Arras D, Rose-John S. IL6 pathway in the liver: from physiopathology to therapy. J Hepatol 2016;64:1403–15.
33. Howlett M, Menheniott TR, Judd LM, Giraud AS. Cytokine signaling via gp130 in gastric cancer. Biochim Biophys Acta 2009;1793:1623–33.
34. Wang B, Kohli J, Demaria M. Senescent cells in cancer therapy: friends or foes? Trends Cancer 2020;6:838–57.
35. Hoare M, Das T, Alexander G. Ageing, telomeres, senescence, and liver injury. J Hepatol 2010;53:950–61.
36. Sharma A, Seow JJW, Dutertre C-A, Pai R, Blériot C, Mishra A, et al. Onco-fetal reprogramming of endothelial cells drives immunosuppressive macrophages in hepatocellular carcinoma. Cell 2020;183:377–94.